J. Appl. Comput. Mech., 5(4) (2019) 763-778
DOI: 10.22055/JACM.2019.27500.1409

ISSN: 2383-4536
jacm.scu.ac.ir

M&MoCS
Shahid Chamran University of Ahvaz

Journal of Applied and Computational Mechanics

Research Paper

Study of MHD Second Grade Flow through a Porous Microchannel under the Dual-Phase-Lag Heat and Mass Transfer Model

Subharthi Sarkar[1], Mehari Fentahun Endalew[1], Oluwole Daniel Makinde[2]

[1] Department of Mathematics, Kalinga Institute of Industrial Technology deemed to be University (KIIT) Bhubaneswar-751024, Odisha, India, Emails: sarkar.ism@gmail.com, mehexf@gmail.com

[2] Faculty of Military Science, Stellenbosch University, Private Bag X2, Saldanha 7395,South Africa, Email: makinded@gmail.com

Received November 01 2018; Revised January 01 2019; Accepted for publication February 08 2019.
Corresponding author: Subharthi Sarkar, sarkar.ism@gmail.com

Abstract. A semi-analytical investigation has been carried out to analyze unsteady MHD second-grade flow under the Dual-Phase-Lag (DPL) heat and mass transfer model in a vertical microchannel filled with porous material. Diffusion thermo (Dufour) effects and homogenous chemical reaction are considered as well. The governing partial differential equations are solved by using the Laplace transform method while its inversion is done numerically using INVLAP subroutine of MATLAB. The numerical values of fluid velocity, fluid temperature and species concentration are demonstrated through graphs while the numerical values of skin friction, heat transfer rate and mass transfer rate presented in tabular form for different values of parameters that govern the flow. For the first time, a comparison of heat transfer utilizing the classical Fourier's heat conduction model, hyperbolic heat conduction Cattaneo-Vernotte (CV) model, and the DPL model is carried out for the flow of a second grade fluid. It is found that the differences between them vanish at dimensionless time t=0.4 (for temperature) and at t=0.5 (for velocity), i.e. at a time where the system reaches steady state. The influence of phase lag parameters in both thermal and solutal transport on the fluid flow characteristics have been deciphered and analyzed. The results conveyed through this article would help researchers to understand non-Fourier heat and mass transfer in the flow of second-grade fluids which may play a vital role in the design of systems in polymer industries.

Keywords: Dual-phase-lag; Double diffusion; Porous Microchannel; MHD second grade flow; Chemical reaction.

1. Introduction

The problems of non-Newtonian fluid have attracted the interest of many scholars due to their important applications in various fields of science, such as glass blowing, crystal growing, oil recovery, food processing, polymer extrusion and many more. Commonly found substances such as salt solutions, ketchup, custard, toothpaste, starch suspensions, honey, paint, blood, shampoo, and molten polymers are non-Newtonian fluids. For other examples of non-Newtonian fluids, one can refer the details about them from the magazine of Ouellette [1]. From these non-Newtonian fluids, our particular emphasis lies upon the second-grade fluids which are very significant in industrial technology. Second-grade magnetohydrodynamics (MHD) flows of viscous incompressible fluids have drawn the attention of many researchers such as Hayat et al. [2, 3] and Hayat and Abbas [4]. Also, the heat and mass transfer of second-grade viscous incompressible fluid is the recent issue of many scholars. Some of the investigators who addressed the issue are Das et al. [5], Babu et al. [6] and Cortell [7].

Moreover, fluids such as liquid metals, plasmas, electrolytes, and salt water are known as magneto-fluids. They have both magnetic property and electrically conducting behaviors. A branch of science that studies such property of fluids, i.e.

Published online: May 09 2019

electrically conducting fluids, combining both principles of fluid dynamics and electromagnetism is called magnetohydrodynamics. Magnetic field plays a very important role in the field of engineering and technology since it is known to control fluid flow in the boundary layer by means of the Lorentz forces and can be effectively used to enhance lift, reduce drag and to suppress any unwanted boundary layer separation. Some important applications are the electromagnetic pump, controlling the cooling of thermonuclear reactors, direct conversion of geothermal energy, flow meters, liquid metal cooling, casting, forging and levitation of metals, heat exchangers. Hence, various investigations could found on MHD flow under different configurations. Some of the recent and significant studies on MHD flows on various flow configurations are made by Sheikholeslami [8- 10], Sheikholeslami *et al*. [11-14], Makinde *et al*. [15-17], Sarkar and Seth [18] and Seth *et al*. [19-21].

In addition, increasing interest for fluid mechanics in microchannel has taken place because of its reasonable applications in numerous biological frameworks where highly effective heat and mass transfer processes take place, for instance, kidneys and lungs. The classification of channel size depends on the perception of a wide range of procedures, yet its utilization is predominant in designating a common terminology. The rate of heat and mass transfer processes in small-diameter channels are also accompanied by a high-pressure drop penalty for fluid flow. The essentials of the microchannel in different applications are introduced in the books of Kandlikar *et al*. [22] and Shen [23]. Moreover, several studies could be found on free convection flow in microchannels. Some of those studies are Misra and Chandra [24], Chen and Weng [25], Hooman [26], Buonomo and Manca [27], Jha *et al*. [28], Hetsroni *et al*. [29] and Das *et al*. [30].

However, the conducted researches so far assumed the classical parabolic diffusion model (Fourier's law of heat conduction model). This model states that the temperature gradient and heat flux vector across a material volume are assumed to happen at the same time instant. The immediate response causes an infinite speed of heat propagation, implying that a thermal disturbance applied at a specific area in a conductor can be detected quickly at any other place within the medium. Since the temperature gradient and heat flux vector are simultaneous, there exists a negligible difference between the cause and the effect of heat flow. Hence, this can be viewed as a direct violation of the theory of causality by Zhang [31]. In addition, this model becomes invalid when we fascinate in the transient heat flow with short time value, small size of space or at very low temperatures, which are essential for the applications such as in cryogenic engineering, material processing using laser beams, electromagnetic irradiation at a solid. Thus, in order to tackle these limitations, the concept of lagging behavior is developed by Conttaneo [32] and Vernotte [33]. This model is known as the thermal wave model or hyperbolic heat conduction model and is a simple modification of classical Fourier's heat conduction model by incorporating relaxation time in the heat flux vector. In the thermal wave or Cattaneo-Vernotte (CV) model, the heat flux vector and the temperature gradient across a material volume are considered to happen at different instants of time. The CV model does avoid the paradox of infinite speed of heat propagation considered in classical Fourier's heat conduction model. However, still it assumes an immediate reply between the energy transport and temperature gradient. This reply happens right after a temperature gradient is created across a material volume; in other words, the thermal wave model assumes an instantaneous heat transport across the same material volume. In the CV model, the temperature gradient is always the cause, while the heat flux vector is always the effect for heat transfer. This assumption has been adapted in the studies by Khadrawi et al. [34] and Choi et al. [35].

Moreover, the DPL model intends to avoid the precedence assumption made in the thermal wave (CV) model. It permits either the temperature gradient (cause) to precede the heat flux vector (effect) or the heat flux vector (cause) to precede the temperature gradient (effect) in the transient process. Mathematically, this can be represented by Tzou [36, 37]:

$$\vec{q}\left(t'+\tau_q^*,\vec{r}\right)=-\kappa\nabla T\left(t'+\tau_T^*,\vec{r}\right) \tag{1}$$

where τ_q^* is the phase lag in the heat flux vector called relaxation time and τ_T^* is the phase lag in the temperature gradient called retardation time. This model is developed by introducing the relaxation time (τ_q^*) in the heat flux vector and retardation time (τ_T^*) in the temperature gradient. When $\tau_T^* > \tau_q^*$, the temperature gradient recorded across a material volume, is a result of the heat flow, which means that the heat flux vector is the cause and the temperature gradient is the effect. On the other hand, when $\tau_T^* < \tau_q^*$, heat flow is induced by the temperature gradient is recorded at an earlier time, implying that the temperature gradient is the cause, while the heat flux vector is the effect. Fundamentals and applications of the model have been discussed by Sobhan and Peterson [38]. When the retardation time vanishes ($\tau_T^* = 0$), the model is reduced to the thermal wave heat conduction model. In the absence of both the relaxation time and retardation time ($\tau_q^* = 0 = \tau_T^*$), the dual phase lagging (DPL) model is reduced to the parabolic classical Fourier's heat conduction model Tzou [37]. Hence, the DPL model is a generalization of all the heat conduction models and its interpretation is more efficient for heat transfer.

So far, the investigations on natural or free convection flow of viscous incompressible fluid utilizing the DPL heat conduction model are very few, making it impossible to cite more. The initial investigation is found by Khadrawi and Al-Nimr [39]. They have investigated time-dependent free or natural convection flow in a vertical microchannel taking the DPL model into account. Afterward, an impressive investigation of the impacts of diffusion-thermo and dual-phase-lag free convection unsteady heat and mass transfer flow in a vertical microchannel filled with porous material is carried out by Ajibade [40]. In his examination, he considered the DPL model for mass transfer as well.

Furthermore, as per the knowledge of authors, no research is conducted on the thermal and solutal behavior of MHD second-grade flow under the effects of dual-phase-lag heat conduction model with diffusion-thermo (Dufour effect) in fully developed flow in a vertical microchannel filled with porous material. This stretches out our inspiration to give more regard for the issue that we have raised and considered. In addition, the effect of the chemical reaction is also taken under consideration.

The influences of various physical parameters on fluid velocity, fluid temperature, fluid concentration, are demonstrated graphically while those of skin friction, heat transfer rate, and mass transfer rate are recorded in tabular form. Using the Laplace transform method, the partial differential equations are transformed into ordinary differential equations and solved. The final solution of the problem has been accomplished by utilizing numerical inversion of the Laplace transform. The results presented in the paper will be bearing in all mechanical systems involving micro-devices and microchannels wherein the dual-phase-lag model provides a better heat and mass transfer analysis.

2. Mathematical Formulation and Solution of the Problem

Consider time-dependent MHD second-grade natural convective flow of viscous incompressible, electrically conducting, and chemically reacting fluid in vertical microchannel filled with porous material. Here, y' axis is assumed to be perpendicular to the microchannel plates which are at a distance h from each other. Initially, the fluid velocity is at rest with initial temperature T_0 and concentration C_0. When $t'>0$, the temperature and concentration at $y'=0$ are raised to T_w and C_w, respectively. The differences in temperature and concentration between the plates induce fluid flow against gravity along the x' direction. A magnetic field (B_o) is applied perpendicular to the flow along the y'-direction. In addition, temperature and concentration jumps, and velocity slip are considered on the channel plates.

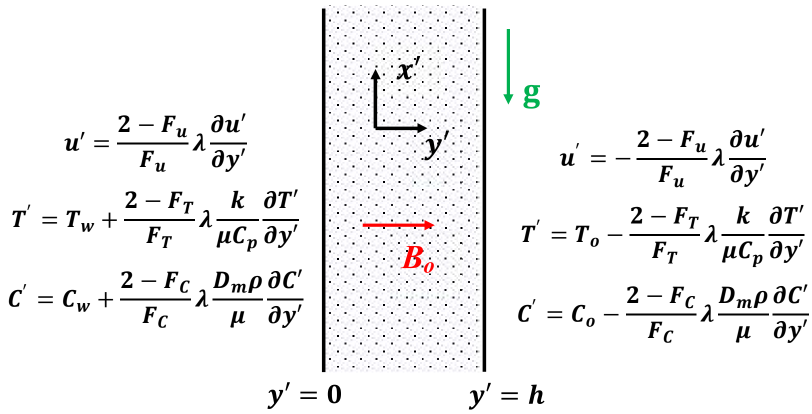

Fig. 1. Geometry of the Problem

It is assumed that the governing equations for temperature and concentration obey the DPL heat conduction model theory. So, we derive the governing equations for temperature and concentration using the concept laid by Tzou [37]. Expanding equation (1) using Taylor series expansion, we get

$$\vec{q} + \tau_q^* \frac{\partial \vec{q}}{\partial t'} = -\kappa\left(\frac{\partial T'}{\partial y'} + \tau_T^* \frac{\partial^2 T'}{\partial t' \partial y'}\right). \tag{2}$$

In the absence of any heat source, Eq. (1) when combined with the energy balance equation gives

$$-\frac{\partial \vec{q}}{\partial y'} = \rho C_p \frac{\partial T'}{\partial t'} \tag{3}$$

By eliminating the heat flux from the equations (2) and (3) and adding the Dufour effect (D_1), we get the heat conduction equation (5). In a similar manner, the dual-phase-lag model for concentration is given in equation (6). The energy dissipations are ignored. Usual Boussinesq's approximation is adopted. The geometrical representation of the problem is given in Fig. 1. Following Hayat et al. [3], Hooman [26], and Ajibade [40], the flow model is given as:

$$\frac{\partial u'}{\partial t'} = \nu_{eff}\frac{\partial^2 u'}{\partial y'^2} + \alpha_1 \frac{\partial^3 u'}{\partial t \partial y'^2} - \left(\frac{\sigma B_o^2}{\rho} + \frac{\nu}{K}\right)u' + g\beta(T' - T_o) + g\tilde{\beta}(C' - C_o), \tag{4}$$

$$\tau_q^* \frac{\partial^2 T'}{\partial t'^2} + \frac{\partial T'}{\partial t'} = \frac{\kappa}{\rho C_p}\left(\frac{\partial^2 T'}{\partial y'^2} + \tau_T^* \frac{\partial^3 T'}{\partial t' \partial y'^2}\right) + D_1 \frac{\partial^2 C'}{\partial y'^2}, \tag{5}$$

$$\lambda_q^* \frac{\partial^2 C'}{\partial t'^2} + \frac{\partial C'}{\partial t'} = D_m\left(\frac{\partial^2 C'}{\partial y'^2} + \lambda_C^* \frac{\partial^3 C'}{\partial t' \partial y'^2}\right) - K_c'(C - C_0), \tag{6}$$

with initial and boundary conditions:

$t' \le 0$:

$$u' = 0, \frac{\partial T'}{\partial t'} = T' = 0, \frac{\partial C'}{\partial t'} = C' = 0, \tag{7a}$$

$t' > 0$:

$$u' = \frac{2-F_u}{F_u}\lambda\frac{\partial u'}{\partial y'},\ T' = T_w + \frac{2-F_T}{F_T}\lambda\frac{k}{\mu C_p}\frac{\partial T'}{\partial y'},\ C' = C_w + \frac{2-F_C}{F_C}\lambda\frac{D_m\rho}{\mu}\frac{\partial C'}{\partial y'},\ at\quad y' = 0 \tag{7b}$$

$$u' = -\frac{2-F_u}{F_u}\lambda\frac{\partial u'}{\partial y'},\ T' = T_0 - \frac{2-F_T}{F_T}\lambda\frac{k}{\mu C_p}\frac{\partial T'}{\partial y'},\ C' = C_0 - \frac{2-F_C}{F_C}\lambda\frac{D_m\rho}{\mu}\frac{\partial C'}{\partial y'},\ at\quad y' = h \tag{7c}$$

where F_u is tangential momentum accommodation coefficient, F_T is thermal accommodation coefficient and F_C is solutal accommodation coefficient. Their values in our study are considered as $F_u = F_T = F_C = 1$. Introducing the following non-dimensional quantities

$$\left.\begin{array}{l} y = \dfrac{y'}{h}, t = \dfrac{t'\nu}{h^2}, T = \dfrac{(T'-T_0)}{(T_w - T_0)}, C = \dfrac{(C'-C_0)}{(C_w - C_0)}, u = \dfrac{u'\nu}{g\beta(T_w - T_0)h^2}, Da = \dfrac{K}{h^2}, Kn = \dfrac{\lambda}{h}, \\ N = \dfrac{\tilde{\beta}(C_w - C_0)}{\beta(T_w - T_0)}, D = \dfrac{D_1(C_w - C_0)}{\alpha(T_w - T_0)}, P_r = \dfrac{\mu C_p}{\kappa}, \tau_T = \dfrac{\tau_T^*\nu}{h^2}, S_c = \dfrac{\nu}{D_m}, \lambda_C = \dfrac{\lambda_C^*\nu}{h^2}, \gamma = \dfrac{\nu_{eff}}{\nu}, \\ \tau_q = \dfrac{\tau_q^*\nu}{h^2}, \lambda_q = \dfrac{\lambda_q^*\nu}{h^2}, M = \dfrac{\sigma B_o^2 h^2}{\rho\nu}, K_c = \dfrac{h^2 K_c'}{\nu}, \alpha = \dfrac{\alpha_1}{\rho h^2} \end{array}\right\} \tag{8}$$

Equations (4-6) are written in dimensional form as

$$\frac{\partial u}{\partial t} = \gamma\frac{\partial^2 u}{\partial y^2} + \alpha\frac{\partial^3 u}{\partial t\,\partial y^2} - \left(M + \frac{1}{Da}\right)u + T + NC, \tag{9}$$

$$\tau_q\frac{\partial^2 T}{\partial t^2} + \frac{\partial T}{\partial t} = \frac{1}{P_r}\left(\frac{\partial^2 T}{\partial y^2} + \tau_T\frac{\partial^3 T}{\partial t\,\partial y^2}\right) + \frac{D}{P_r}\frac{\partial^2 C}{\partial y^2}, \tag{10}$$

$$\lambda_q\frac{\partial^2 C}{\partial t^2} + \frac{\partial C}{\partial t} = \frac{1}{S_C}\left(\frac{\partial^2 C}{\partial y^2} + \lambda_C\frac{\partial^3 C}{\partial t\,\partial y^2}\right) - K_c C. \tag{11}$$

Subject to initial and boundary conditions

$t \le 0$:

$$u = 0, \frac{\partial T}{\partial t} = T = 0, \frac{\partial C}{\partial t} = C = 0, \tag{12a}$$

$t > 0$:

$$u = Kn\frac{\partial u}{\partial y},\ T = 1 + \frac{Kn}{P_r}\frac{\partial T}{\partial y},\ C = 1 + \frac{Kn}{S_C}\frac{\partial C}{\partial y}\ at\quad y = 0 \tag{12b}$$

$$u = -Kn\frac{\partial u}{\partial y},\ T = -\frac{Kn}{P_r}\frac{\partial T}{\partial y},\ C = -\frac{Kn}{S_C}\frac{\partial C}{\partial y}\ at\quad y = 1 \tag{12c}$$

Taking the Laplace transform on equations (9-12) we get the following ordinary differential equations.

$$\frac{d^2\tilde{u}}{dy^2} - R\tilde{u} = -(\tilde{T} + N\tilde{C})(\gamma + s\alpha)^{-1}, \tag{13}$$

$$\frac{d^2\tilde{T}}{dy^2} - P\tilde{T} = \frac{-Dq}{1 + s\tau_T}\tilde{C}, \tag{14}$$

$$\frac{d^2\tilde{C}}{dy^2} - q\tilde{C} = 0, \tag{15}$$

where $R=(sDa+MDa+1)(Da(\gamma+s\alpha))^{-1}$, $P=P_r(s+s^2\tau_q)(1+s\tau_T)^{-1}$, $q=S_c(K_c+s+s^2\lambda_q)(1+s\lambda_C)^{-1}$, while the boundary conditions are transformed as follows

$$\tilde{u}=Kn\frac{d\tilde{u}}{dy},\ \tilde{T}=\frac{1}{s}+\frac{Kn}{P_r}\frac{d\tilde{T}}{dy},\ \tilde{C}=\frac{1}{s}+\frac{Kn}{S_C}\frac{d\tilde{C}}{dy}\qquad at\quad y=0, \tag{16a}$$

$$\tilde{u}=-Kn\frac{d\tilde{u}}{dy},\ \tilde{T}=-\frac{Kn}{P_r}\frac{d\tilde{T}}{dy},\ \tilde{C}=-\frac{Kn}{S_C}\frac{d\tilde{C}}{dy}\qquad at\quad y=1. \tag{16b}$$

The solutions for equations (13-15) are as follows

$$\tilde{u}=C_1e^{-y\sqrt{R}}+C_2e^{y\sqrt{R}}+C_3e^{-y\sqrt{P}}+C_4e^{y\sqrt{P}}+C_5e^{y\sqrt{q}}+C_6e^{-y\sqrt{q}}, \tag{17}$$

$$\tilde{T}=B_1e^{-y\sqrt{P}}+B_2e^{y\sqrt{P}}+B_3e^{y\sqrt{q}}+B_4e^{-y\sqrt{q}}, \tag{18}$$

$$\tilde{C}=A_1e^{y\sqrt{q}}+A_2e^{-y\sqrt{q}}. \tag{19}$$

All the physical parameters and constants are defined in the nomenclature and appendix. The inversion of expressions (17-19) should be performed in order to obtain the velocity, temperature and concentration in the time domain. To achieve this, the method of numerical inversion of the Laplace transform is employed, since the Laplace inverse of the above solutions (17-19) do not admit closed-form analytical solutions in the time domain. Therefore, we use the INVLAP subroutine of MATLAB [42] based on De Hoog's algorithm [41] for numerical inversion of transformed equations (17-19). The numerical inversion of the Laplace transform (INVLAP) is shown in the following flow chart (Chart 1).

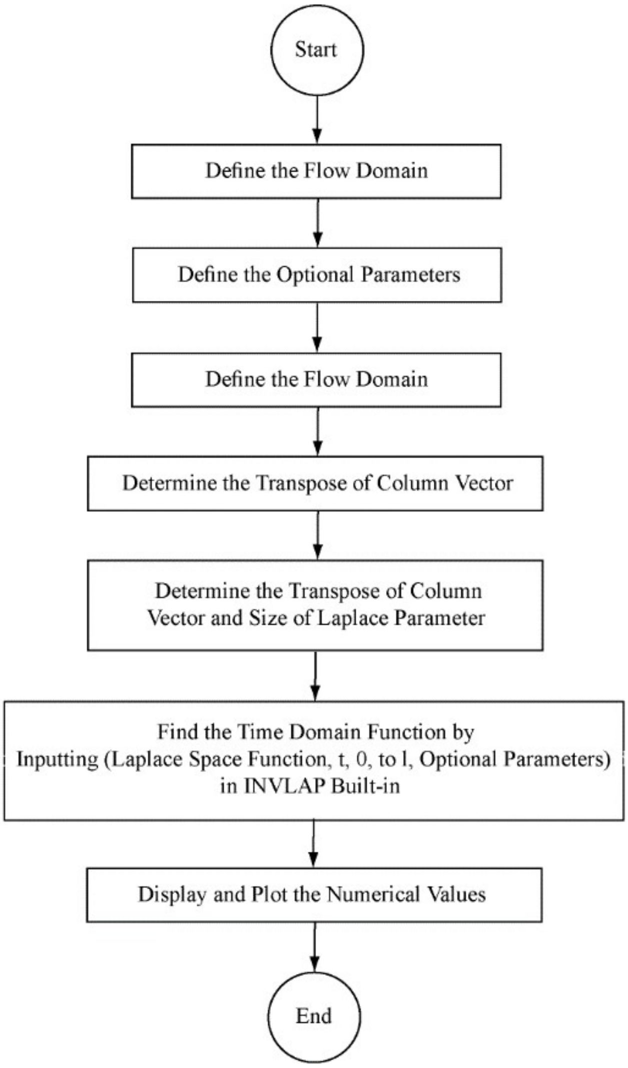

Chart 1. Flowchart depicting the numerical method using the INVLAP subroutine of MATLAB

The validity of our numerical result is compared by taking ($K_C=M=\alpha=0$) with existing solution of Ajibade [40] (see Fig. 2) and it is found in good agreement.

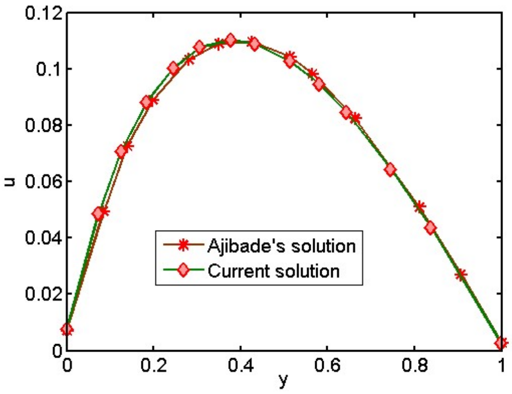

Fig. 2. Validity of numerical result

Next, the very curial quantities in the fluid flow, i.e. skin friction, heat and mass transfer rates can be derived as follows.

Skin friction:

Local skin friction is obtained from equation (17) and is written as

$$\tau_0 = \left.\frac{\partial \tilde{u}(y,s)}{\partial y}\right|_{y=0} = \sqrt{R}(C_2 - C_1) + \sqrt{P}(C_4 - C_3) + \sqrt{q}\left(C_6 - C_5\right) \tag{20a}$$

$$\tau_1 = \left.\frac{\partial \tilde{u}(y,s)}{\partial y}\right|_{y=1} = \sqrt{R}(C_2 e^{\sqrt{R}} - C_1 e^{-\sqrt{R}}) + \sqrt{P}(C_4 e^{\sqrt{P}} - C_3 e^{-\sqrt{P}}) + \sqrt{q}\left(C_6 e^{\sqrt{q}} - C_5 e^{-\sqrt{q}}\right). \tag{20b}$$

Heat transfer rate (Nusselt Number):

Heat transfer rate is obtained from equation (18) and is written as:

$$Nu_0 = \left.\frac{\partial \tilde{T}(y,s)}{\partial y}\right|_{y=0} = \sqrt{P}(B_2 - B_1) + \sqrt{q}(B_4 - B_3), \tag{21a}$$

$$Nu_1 = \left.\frac{\partial \tilde{T}(y,s)}{\partial y}\right|_{y=1} = \sqrt{P}(B_2 e^{\sqrt{P}} - B_1 e^{-\sqrt{P}}) + \sqrt{q}(B_4 e^{\sqrt{q}} - B_3 e^{-\sqrt{q}}). \tag{21b}$$

Mass transfer rate (Sherwood number):

Mass transfer rate is obtained from the equation (19) and is written as:

$$Sh_0 = \left.\frac{\partial \tilde{C}(y,s)}{\partial y}\right|_{y=0} = \sqrt{q}(A_1 - A_2), \qquad Sh_1 = \left.\frac{\partial \tilde{C}(y,s)}{\partial y}\right|_{y=1} = \sqrt{q}(A_1 e^{\sqrt{q}} - A_2 e^{-\sqrt{q}}). \tag{22}$$

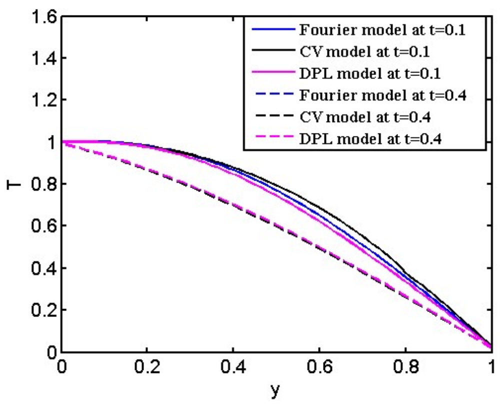

Fig. 3a Temperature profiles of different models

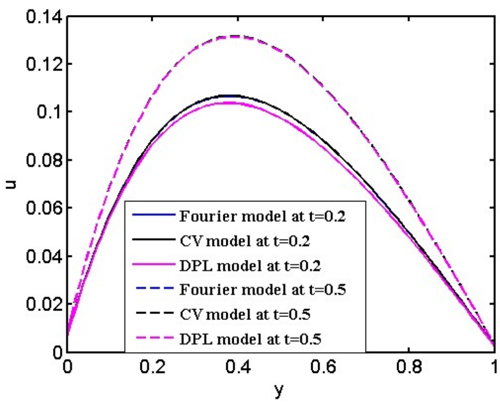

Fig. 3b Velocity profiles of different models

To get the solution for skin friction, heat transfer rate and mass transfer rate, we invert equations (20-22) by using INVLAP-routine of MATLAB. It is worthy to note that the solution of the present problem encompasses all the models since for $\tau_q = \tau_T = \lambda_q = \lambda_C = 0$, the solution reduces to classical parabolic heat conduction (Fourier's) model, for $\tau_T = \lambda_C = 0$, hyperbolic heat conduction (CV) model and for $\tau_q = \tau_T = \lambda_q = \lambda_C \neq 0$ it gives the dual phase lag model. So, for the first time, the comparisons of those models (classical Fourier's heat conduction model), hyperbolic heat conduction (CV) model and DPL model) are carried out for different values of time. It is found from Figs.3a and 3b that as time increases, the difference between these models reduces. That is, fluid temperature recorded using the different models (for this problem) becomes the same beyond *t*=0.4. The same thing happens for fluid velocity beyond *t*=0.5. Hence, in this problem, for the simulation purposes, we have fixed time *t*=0.1, so that the actual results specific to the DPL model could be produced.

3. Results and Discussion

Non-dimensional fluid velocity, fluid temperature, species concentration are presented in Figs. 4–37 while skin friction, heat transfer rate and mass transfer rate are put in view in Tables 1-3 for the various fundamental physical parameters. In this study, Dual-Phase-Lag of both heat and mass transfer on MHD second grade flow in a porous microchannel are discussed. Here, we try to capture the subtle and transient features in fluid flow and heat and mass transfer characteristics for various values of pertinent flow parameters amidst the lagging response in the transfer of heat and solute. In the computation of numerical results in this article, unless otherwise stated, the following important parameters are used $Da = 0.1,\ M = 1,\ \tau_q = 0.001,\ \tau_T = 0.01,\ Kc = 1\ \lambda_q = 0.001,\ \lambda_C = 0.01,\ Sc = 0.66,\ Kn = 0.01,\ \Pr = 0.71,\ \gamma = 1,\ D = 2,\ N = 2,$ $\alpha = 0.1$ and $t = 0.1$.

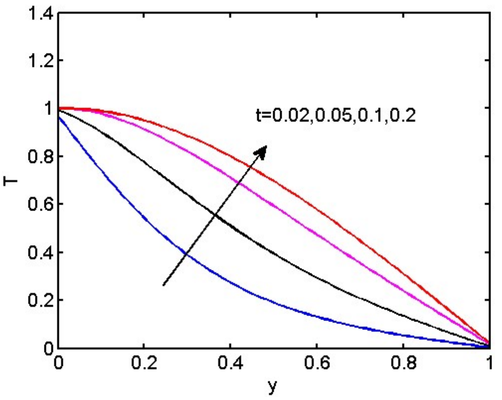

Fig. 4. Temperature profiles for values of *t*

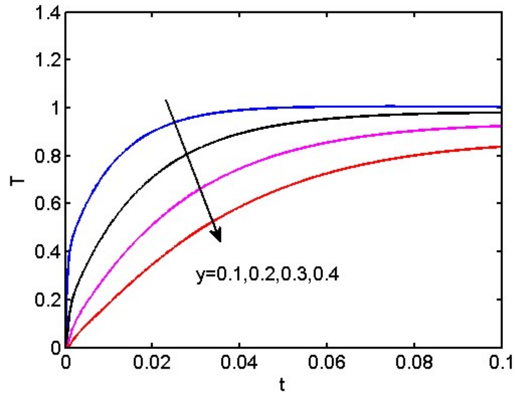

Fig. 5. Temperature profiles for values of *y*

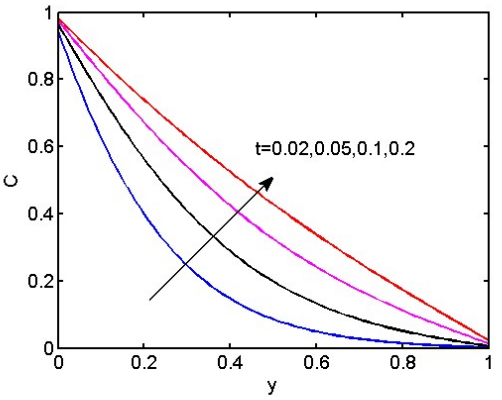

Fig. 6. Concentration profiles for values of *t*

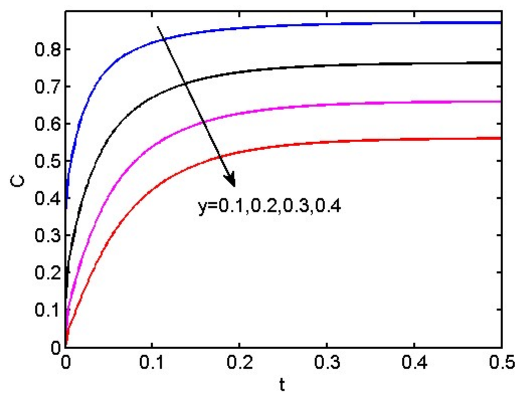

Fig. 7. Concentration profiles for values of *y*

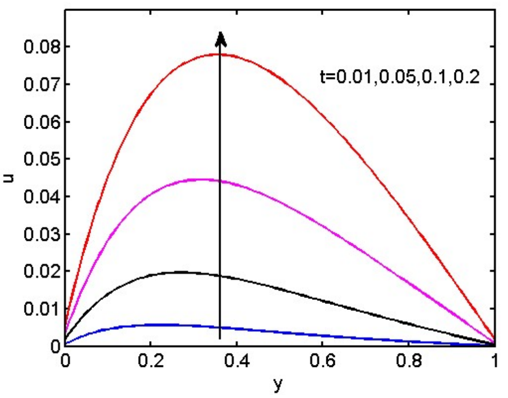

Fig. 8. Velocity profiles for different values of *t*

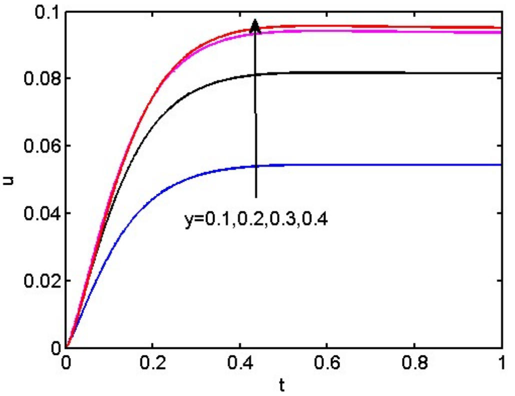

Fig. 9. Velocity profiles for different values of *y*

The variation of fluid temperature spatial distribution in the microchannel with respect to time and space are presented in the

Figs. 4 and 5. From these records, we can observe that fluid temperature increases with the passage of time whereas it reduces as space size y becomes larger. Physically speaking, this happens because heat flow is directly proportional to the change of temperature and inversely proportional to the distance between the ends of heat sources. Hence, lowering of temperature is observed as distance y increases. Figs. 6 and 7 display the time and space variation of species concentration. Species concentration increases with time and decreases with space coordinate. This is because the gradient of species concentration is the quotient of the difference of concentration and the distance between the ends. Thus, species concentration moves down as distance rise up whereas it increases by increasing time.

Figs. 8 and 9 depict the feature of fluid velocity under the time and space coordinates. As we expected, the fluid velocity rises with respect to time and along the space. Figs. 10, 11 and 12 display the influence of Knudsen number on the fluid temperature, fluid concentration and fluid velocity. Knudsen number represents the ratio of molecular mean free path to characteristic physical length of microchannel. Thus, when Knudsen number (Kn) increases, molecules mean free path will increase. This results in the less chance of contact among the molecules in the channel. In addition, a higher Knudsen number implies fewer molecules will collide with the wall. Hence, due to less collision, there would be less heat generated and less energy transfer as well. This is why fluid temperature reduces as Kn increases (Fig. 10). In fact, the maximum temperature at y=1 also reduces with the increase in Kn. Similar argument works well for species concentration because mass transfer reduces due to fewer collisions upon the increase of Kn. It is seen from Fig. 12 that species concentration reduces as Kn increases. Fluid velocity increases with Kn (near the source plate y=0) in the channel and carries a part of its heating effect. As a result of an expansion of temperature jump at the wall of the channel, little heat is spread into the fluid, and the buoyancy force became less. Hence, the fluid temperature decreases as Kn increases. The same aspect is observed for the fluid concentration. As Kn increases, temperature and concentration decrease. This causes the expansion of the fluid velocity due to the buoyancy effect.

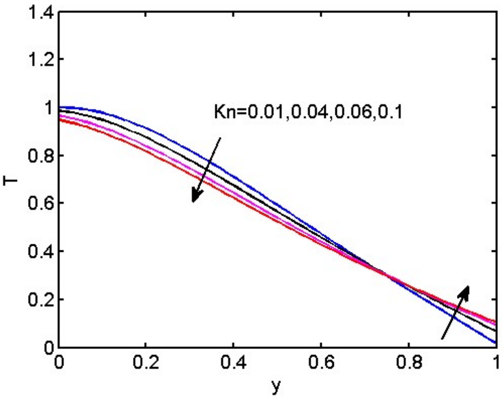

Fig. 10. Temperature profiles for different values of Kn

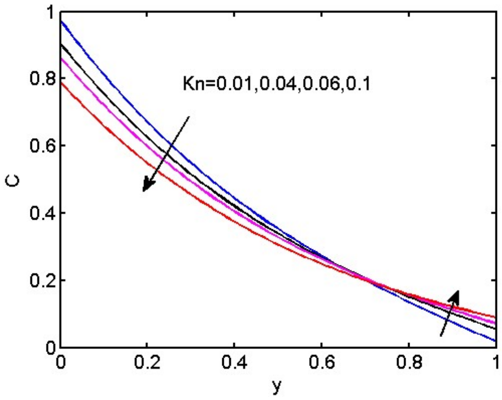

Fig. 11. Concentration profiles for different values of Kn

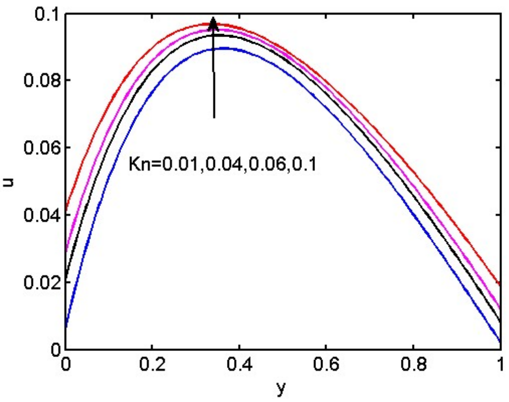

Fig. 12. Velocity profiles for different values of Kn

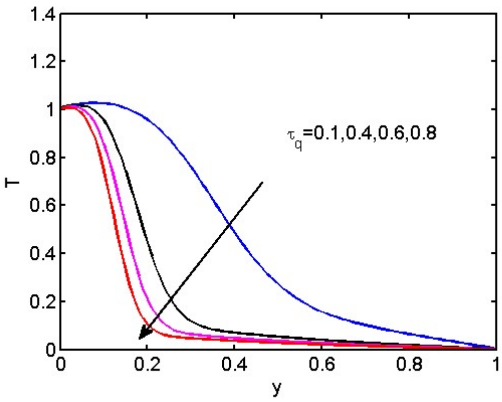

Fig. 13. Temperature profiles for different values of τ_q

Figs. 13 and 14 exhibit the impact of thermal relaxation time (τ_q) on the fluid temperature and fluid velocity. Here, we can see that both velocity and temperature profiles fall down as thermal relaxation time (τ_q) increases. When thermal relaxation time increases, the cooling tendency of fluid within the channel is higher, this causes the reduction of temperature distribution and velocity. Figs. 15 and 16 show the impact of thermal retardation time (τ_T) on the fluid temperature and flow velocity profiles for the given time. From these figures, anybody can see that the fluid velocity and temperature are decreasing as retardation time increases. Obviously, when retardation time increases with length of time, the response of thermal force is delayed to propagate. Due to this fact, both quantities are decreasing with the increase in retardation time. The influence of the phase lag in the mass flux (λ_q) on the fluid temperature, chemical concentration and fluid velocity are exposed in Figs. 17, 18 and 19. Species concentration and fluid velocity profiles decrease with increase of phase lag in the mass flux. However, fluid temperature profiles increase with the expansion of phase lag in the mass flux.

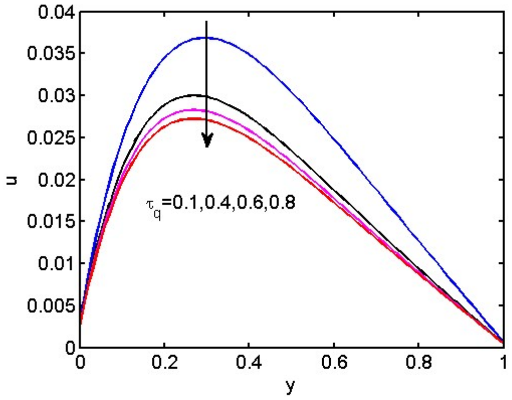

Fig. 14. Velocity profiles for different values of τ_q

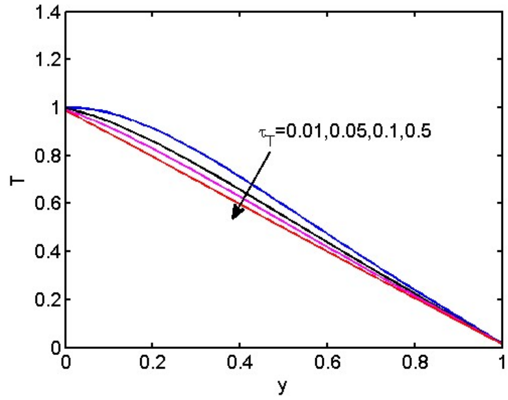

Fig. 15. Temperature profiles for different values of τ_T

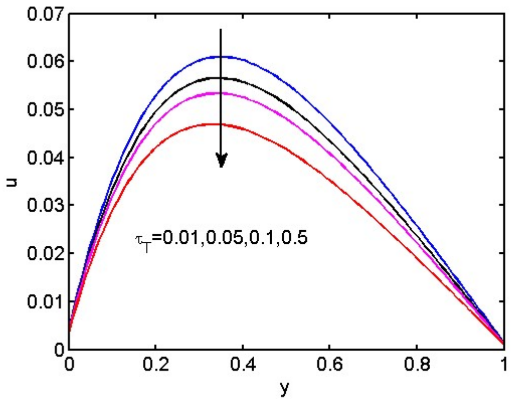

Fig. 16. Velocity profiles for different values of τ_T

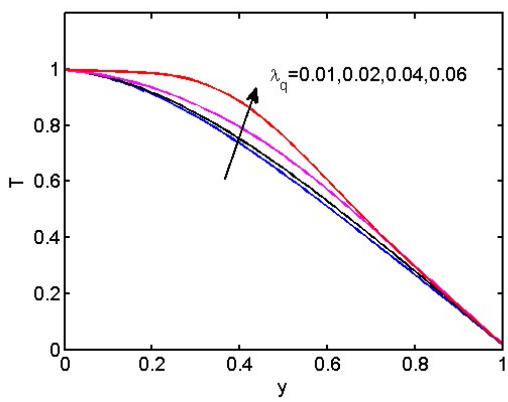

Fig. 17. Temperature profiles for different values of λ_q

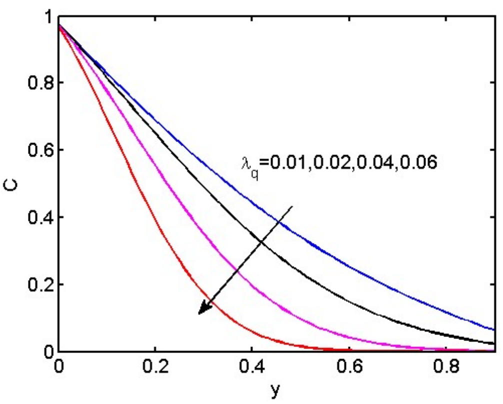

Fig. 18. Concentration profiles for different values of λ_q

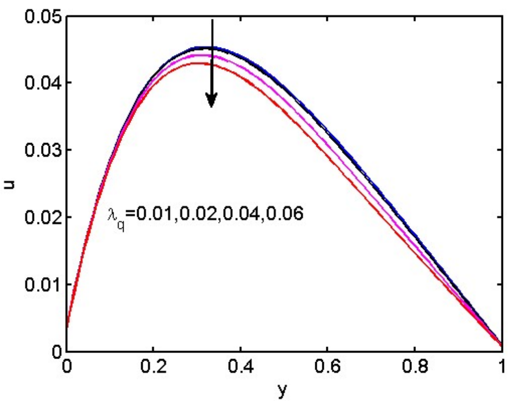

Fig. 19. Velocity profiles for different values of λ_q

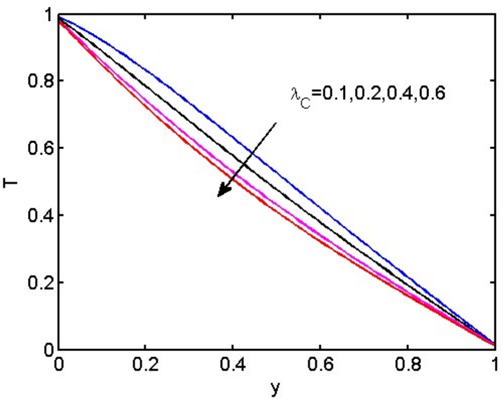

Fig. 20. Temperature profiles for different values of λ_C

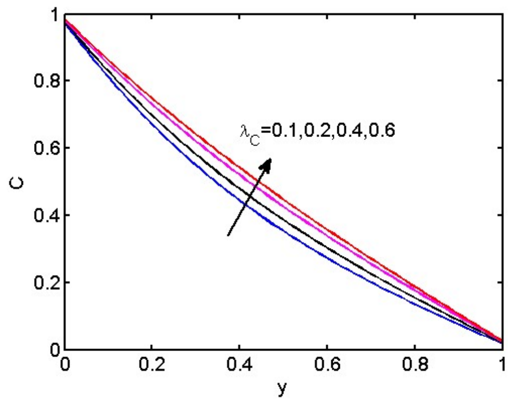

Fig. 21. Concentration profiles for different values of λ_C

The impact of the phase lag in the concentration gradient (λ_C) on the fluid temperature, chemical concentration and fluid velocity are revealed in Figs. 20, 21 and 22, respectively. Species concentration and fluid velocity profiles increase with the increase of phase lag in the concentration gradient. However, temperature profiles diminish as phase lag in concentration gradient increases through the microchannel. The impact of Dufour number on the fluid temperature and fluid velocity is portrayed in Figs. 23 and 24, respectively. Dufour number is a dimensionless parameter used to study thermo-diffusion. It signifies the ratio of increase in enthalpy of a unit mass during isothermal mass transfer to the enthalpy of a unit mass of the mixture. Increasing the Dufour number enforces to a growth in the energy flux due to molecular diffusion. This directs to an augmentation of the fluid temperature. Consequently, molecules move faster in the microchannel, which yields an increase in fluid velocity.

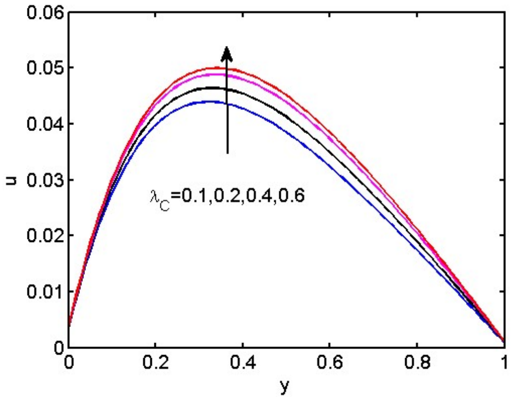

Fig. 22. Velocity profiles for different values of λ_C

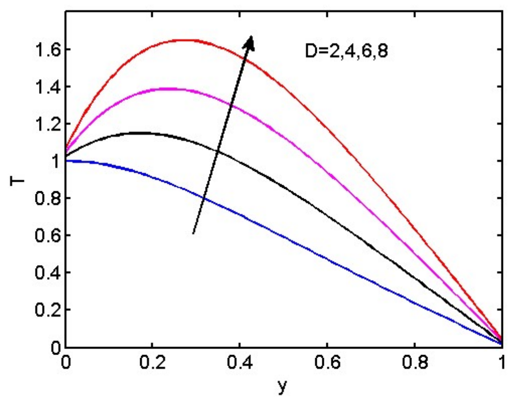

Fig. 23. Temperature profiles for different values of D

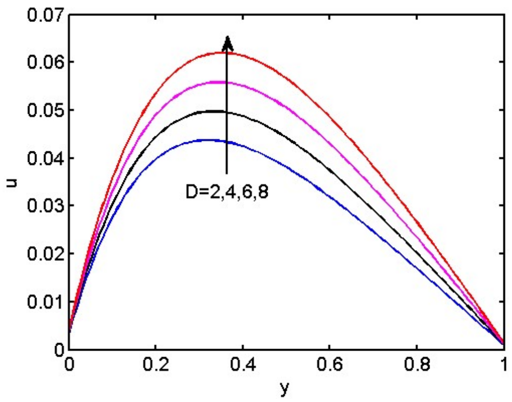

Fig. 24. Velocity profiles for different values of D

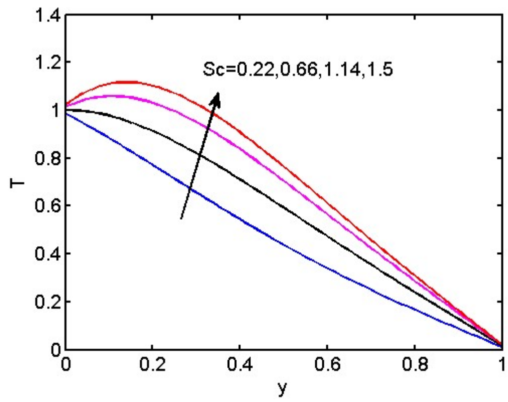

Fig. 25. Temperature profiles for different values of Sc

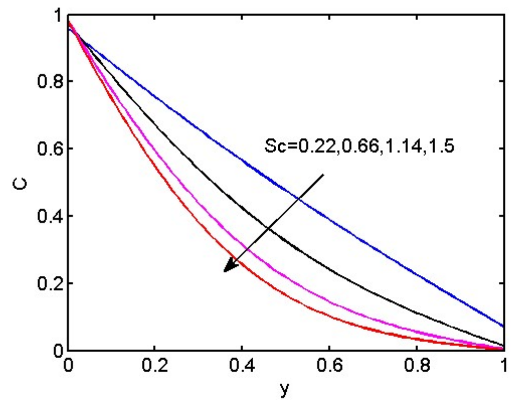

Fig. 26. Concentration profiles for different values of Sc

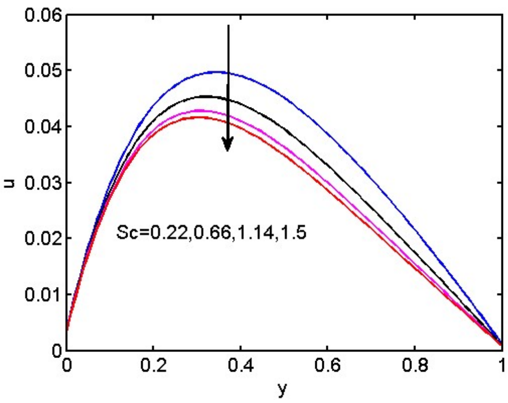

Fig. 27. Velocity profiles for different values of Sc

Figs. 25, 26 and 27 display the influence of Schmidt number on the fluid temperature, species concentration and fluid velocity profiles in the microchannel. Physically, the Schmidt number is a dimensionless number that represents the ratio of kinematic viscosity to molecular/mass diffusivity. Hence an increment in molecular diffusivity causes a reduction in the value of Schmidt number. It is very important to characterize fluid flow in which there are simultaneous momentum and mass diffusion convection process. In short, it describes the mass momentum transfer. Typical values for the Schmidt number are chosen at the room temperature and assigned as, for the helium (He) ($Sc = 0.22$), water (H_2O) ($Sc = 0.66$), methanol ($Sc = 1.14$) and ethanol ($Sc = 1.5$). Here, both species concentration and fluid velocity decrease with increasing the values of Schmidt number. It is obvious from the fact that when the Schmidt number increases; the viscous force dominates the flow, which leads to the cutback of fluid velocity and molecular diffusion enforced to be less, yields that the diminution of the fluid concentration. However, when the Schmidt number rises, the thickness of boundary layer becomes smaller. This results in the increase of the fluid temperature within the microchannel. Figs. 28, 29 and 30 show the effect of the chemical reaction parameter on the fluid temperature, species concentration and fluid velocity. From these figures, we can see that the fluid concentration and the fluid velocity decrease with the increase of chemical reaction parameter. The temperature distribution increases with the increase of chemical reaction parameter. This is due to the presence of more thermal energy available to reach the activation energy to compensate the breaking of bonds between atoms.

Figs. 31 and 32 depict the influence of Prandtl number on the temperature and fluid velocity at the smaller time and larger time, respectively. Prandtl number is a dimensionless number (named after a physicist Ludwig Prandtl). Physically, it is the ratio of viscosity to the thermal diffusivity. That is, as thermal diffusivity increases, Prandtl number reduces. In our numerical simulation, we tried to compare thermal diffusivity of water and air at the room temperature. Hence, the species chosen in our simulation are, (air at the room temperature (Pr = 0.71), gaseous ammonia at the room temperature (Pr =1.38), water at the room temperature (Pr =7) and water vapor at $4^{o}C$ (Pr = 11.66). Here, we can observe that the thermal diffusivity is more dominant for air than water at room temperature. However, the thermal diffusivity of gaseous ammonia at the room temperature is higher than water vapor. It is seen that the fluid velocity and temperature distribution experience considerable shrinking for expanding estimations of Prandtl number. This is due to the fact that, increasing Prandtl number causes reduction of the thermal diffusivity and expansion of frictional force. Hence, both fluid velocity and temperature decrease as Prandtl number increases at any time. In addition, the thickness of the thermal boundary layer reduces as thermal diffusivity decreases.

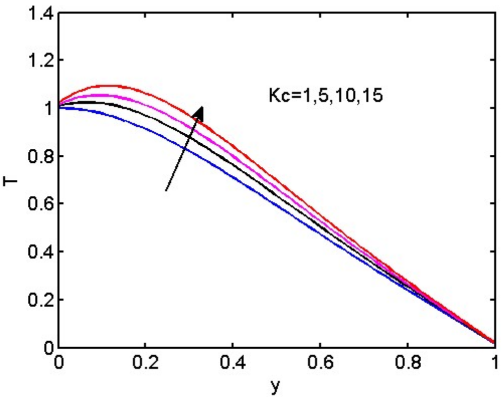

Fig. 28. Temperature profiles for different Kc

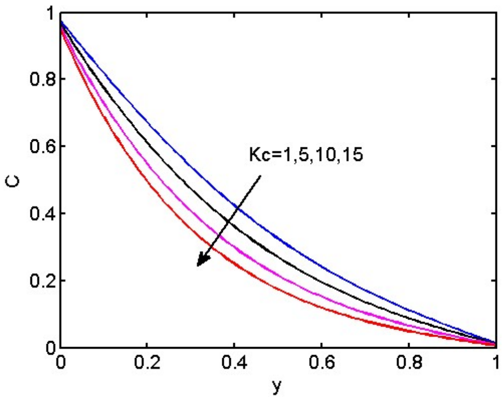

Fig. 29. Concentration profiles for different Kc

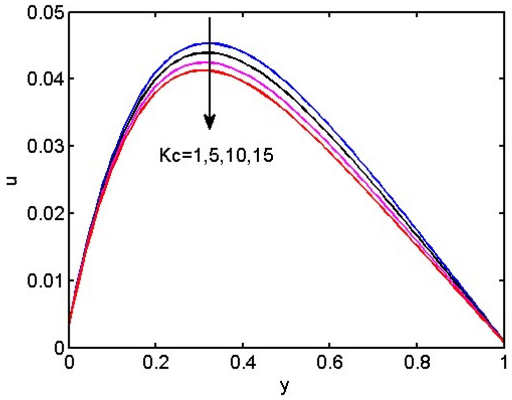

Fig. 30. Velocity profiles for different values of Kc

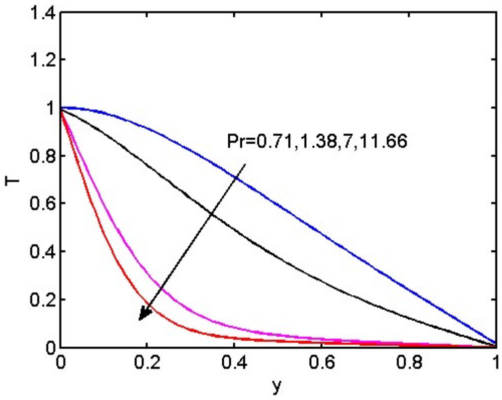

Fig. 31. Temperature profiles for different values of Pr

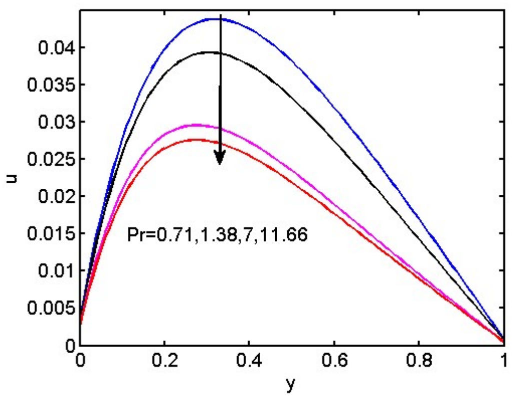

Fig. 32. Velocity profiles for different values of Pr

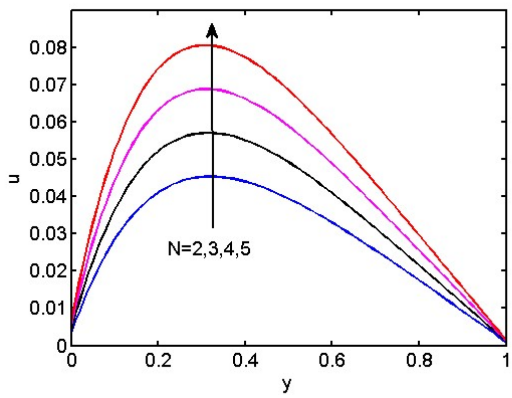

Fig. 33. Velocity profiles for different values of N

The influence of sustention parameter on the fluid velocity is represented in Fig. 33. Physically speaking, sustention parameter is the ratio of solutal buoyancy force to the thermal buoyancy force. Hence, the increase of sustention parameter causes domination of solutal buoyancy force in the fluid for our choice ($N \geq 2$), and yields the quick diffusing of species. Thus, the presence of more solutal buoyancy force entails the fluids to move easily and quickly. Hence, the fluid velocity increases with increasing sustention parameter as expected. Fig. 34 shows the effect of Darcy number on the velocity profiles. Darcy number is the quotient of permeability of medium and cross-sectional area. Due to this, as permeability increases the fluid can move quickly. Hence, fluid velocity increases as Darcy number increases. This is due to an expansion of permeability of a channel, which yields faster passage of flow within the microchannel.

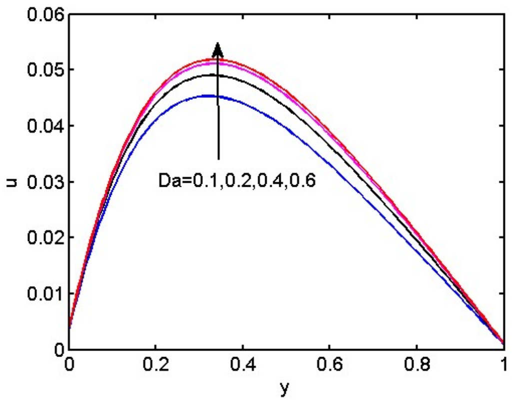

Fig. 34. Velocity profiles for different values of Da

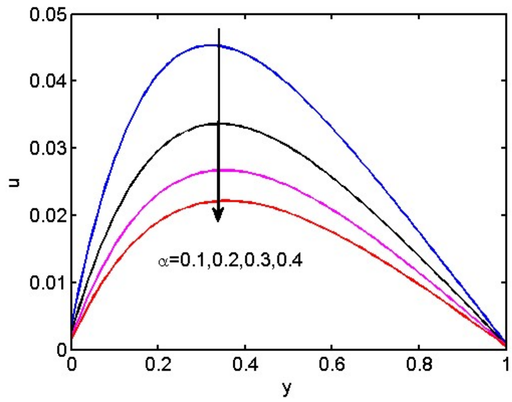

Fig. 35. Velocity profiles for different values of α

When the second-grade parameter (α) expands, the apparent thickness of the fluid will become more burdensome (the flow is dominated by viscous/frictional force). Due to this, increasing the second-grade parameter provides extra thickness of the boundary surface of the channel. Therefore, an increment in the second parameter provides more friction and hence diminishes the fluid velocity as shown in Fig. 35. From Fig. 36, it is seen that fluid velocity diminishes as the magnetic parameter ascends. Physically speaking, the magnetic field generates a Lorentz force which slows down the fluid's motion. Hence, the fluid velocity diminishes as the magnetic field parameter increases. Also, it is similar to the increase in viscosity ratio, i.e. fluid flow with under high M behaves like a flow of high viscous fluids (low velocity) and this could be easily comprehended by comparing the Figs. 36 and 37. In common knowledge, viscosity is the ability of measuring a fluid's resistance to flow. Due to this fact, the fluid velocity decreases as the viscosity ratio (γ) increases.

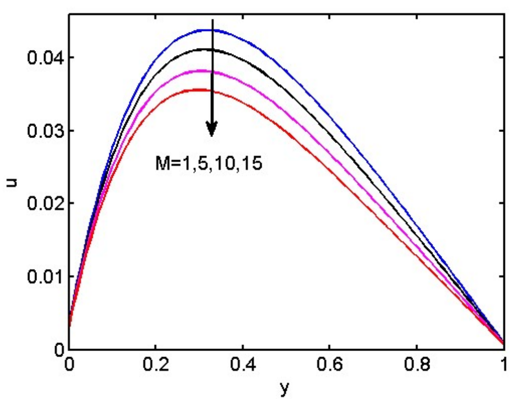

Fig. 36. Velocity profiles for different values of M

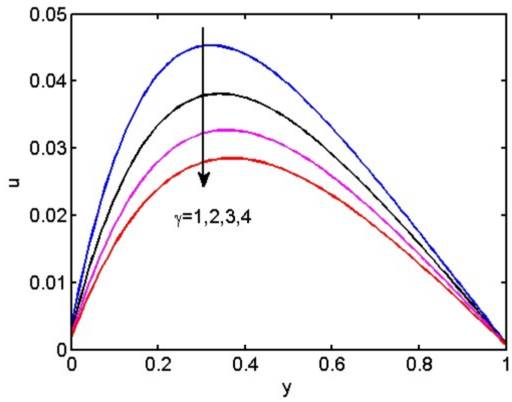

Fig. 37. Velocity profiles for different values of γ

Tables 1-3 show the records of variation of heat transfer rate, the variation of mass transfer rate, and variation of skin friction of the problem for various pertinent physical parameters, respectively. Table 1 displays the influence of pertinent parameters on the heat transfer rate (Nusselt number) at $y=0$ and $y=1$. From these records at $y=0$, we can observe that the heat transfer rate at the wall $y=0$ (Nu_0) decreases in magnitude as $Kc, Sc, \tau_q, D, \lambda_C$ and t increase. However, there the heat transfer rate increases in magnitude with an increase in $Kn, \Pr, \tau_T$ and λ_q. That is heat transfer rate at the wall $y=0$ diminishes in its magnitude with an increase in the chemical reaction parameter, thermal diffusivity, thermal relaxation, thermo-diffusion, phase lag in concentration, and time whereas heat transfer rate enhances as mean free path of molecules, molecular diffusivity, thermal retardation time, and phase lag in mass flux increase. Heat transfer rate at the wall $y=1$, (Nu_1) increases in magnitude with an increase in $Kc, Sc, \tau_q, D, \lambda_q$ and t rise and diminishes in magnitude as $Kn, \Pr, \tau_T$ and λ_C rise. That is, heat transfer rate at the wall, $y=1$, increases in its magnitude as chemical reaction, thermal diffusivity, thermal relaxation time, thermo-diffusion, phase lag in mass flux, and time. But it diminishes with increase in mean free path of molecules, molecular diffusivity, thermal retardation time and phase lag in concentration. The influence of important physical parameters on the mass transfer rate is presented in Table 2. Here, we can see that at $y=0$, mass transfer rate (Sh_0) reduces in magnitude with the rise of Kn, λ_q, t and rises in magnitude as Kc, Sc and λ_C rise. On the other hand, except Knudsen number (Kn), which causes an increase in mass transfer rate with its expansion; other physical parameters show the opposite effect on the mass transfer rate (Sh_1) at the wall of channel (y = 1).That is, the chemical reaction parameter, Schmidt number, phase-lags in mass flux and concentration exhibit opposite impacts on the mass transfer rate at the wall $y = 1$.

Table 1. Variation of heat transfer rate

t	Kn	τ_q	τ_T	λ_q	λ_C	D	Kc	Sc	Pr	$-Nu_0$	Nu_1
0.1	0.01	0.001	0.01	0.001	0.01	1	1	0.66	0.71	0.713	0.978
0.2	0.01	0.001	0.01	0.001	0.01	1	1	0.66	0.71	0.627	1.209
0.1	0.02	0.001	0.01	0.001	0.01	1	1	0.66	0.71	0.717	0.927
0.1	0.06	0.001	0.01	0.001	0.01	1	1	0.66	0.71	0.750	0.733
0.1	0.01	0.002	0.01	0.001	0.01	1	1	0.66	0.71	0.705	0.980
0.1	0.01	0.01	0.01	0.001	0.01	1	1	0.66	0.71	0.643	0.998
0.1	0.01	0.001	0.02	0.001	0.01	1	1	0.66	0.71	0.742	0.952
0.1	0.01	0.001	0.06	0.001	0.01	1	1	0.66	0.71	0.887	0.907
0.1	0.01	0.001	0.01	0.002	0.01	1	1	0.66	0.71	0.716	0.983
0.1	0.01	0.001	0.01	0.01	0.01	1	1	0.66	0.71	0.742	1.029
0.1	0.01	0.001	0.01	0.001	0.02	1	1	0.66	0.71	0.673	0.934
0.1	0.01	0.001	0.01	0.001	0.06	1	1	0.66	0.71	0.649	0.834
0.1	0.01	0.001	0.01	0.001	0.01	1.1	1	0.66	0.71	0.629	1.029
0.1	0.01	0.001	0.01	0.001	0.01	1.5	1	0.66	0.71	0.295	1.231
0.1	0.01	0.001	0.01	0.001	0.01	1	2	0.66	0.71	0.533	1.031
0.1	0.01	0.001	0.01	0.001	0.01	1	4	0.66	0.71	0.347	1.036
0.1	0.01	0.001	0.01	0.001	0.01	1	1	0.22	0.71	1.204	0.735
0.1	0.01	0.001	0.01	0.001	0.01	1	1	1.5	0.71	0.279	1.109
0.1	0.01	0.001	0.01	0.001	0.01	1	1	0.66	0.9	0.974	0.753
0.1	0.01	0.001	0.01	0.001	0.01	1	1	0.66	1	2.545	0.169

Table 2. Variation of mass transfer rate

t	Kn	λ_q	λ_C	Kc	Sc	$-Sh_0$	$-Sh_1$
0.1	0.01	0.001	0.01	1	0.66	1.624	0.455
0.2	0.01	0.001	0.01	1	0.66	1.284	0.737
0.1	0.02	0.001	0.01	1	0.66	1.608	0.400
0.1	0.06	0.001	0.01	1	0.66	1.534	0.255
0.1	0.01	0.002	0.01	1	0.66	1.619	0.456
0.1	0.01	0.01	0.01	1	0.66	1.576	0.454
0.1	0.01	0.001	0.02	1	0.66	1.685	0.469
0.1	0.01	0.001	0.06	1	0.66	1.824	0.522
0.1	0.01	0.001	0.01	2	0.66	1.748	0.427
0.1	0.01	0.001	0.01	4	0.66	1.985	0.376
0.1	0.01	0.001	0.01	1	0.22	1.047	0.762
0.1	0.01	0.001	0.01	1	1.5	2.440	0.127

Table 3 shows the variation of local skin friction at $y = 0$ and $y = 1$ for several important physical parameters. Here, we can see that skin friction at $y = 0$ (τ_0) increases with the increment of $Da, D, K_c, \lambda_q, \lambda_C$ and time t. However, with the increase in $N, M, Sc, Kn, \Pr, \tau_q, \tau_T, \gamma$ and α skin friction τ_0 decreases. That is, the magnitude of local skin friction at wall $y = 0$ rises with an increase in Darcy number, thermo-diffusion, chemical reaction, phase-lags in mass flux and concentration, time and thermal and molecular diffusivity whereas it diminishes with an increment of sustention parameter, magnetic field parameter, mean free path of molecules, thermal retardation time, thermal relaxation time, viscosity ratio and second grade parameter. On the other hand, skin friction at the wall $y = 1$ (τ_1) increases in magnitude with an increase in D, N, Da, Kc, λ_C and time t and it decreases in magnitude as $Sc, Kn, \Pr, \tau_q, M, \gamma, \tau_T, \lambda_q$ and α increase. Hence, skin friction in its magnitude at the wall ($y = 1$) increases with an increase in thermo-diffusion, sustention parameter, Darcy number, chemical reaction, phase lag in concentration, time and thermal and molecular diffusivity whereas it reduces as mean free path of molecules, thermal retardation time, magnetic field parameter, thermal retardation time, viscosity ratio, phase lag in mass flux and second grade parameter increase.

Table 3. Variation of skin friction

t	Kn	τ_q	τ_T	λ_q	λ_C	D	Kc	Sc	Pr	N	Da	M	γ	α	τ_0	$-\tau_1$
0.1	0.01	0.001	0.01	0.001	0.01	2	1	0.66	0.71	2	0.1	1	1	0.1	0.332	0.084
0.2	0.01	0.001	0.01	0.001	0.01	2	1	0.66	0.71	2	0.1	1	1	0.1	0.514	0.169
0.1	0.02	0.001	0.01	0.001	0.01	2	1	0.66	0.71	2	0.1	1	1	0.1	0.312	0.081
0.1	0.06	0.001	0.01	0.001	0.01	2	1	0.66	0.71	2	0.1	1	1	0.1	0.249	0.069
0.1	0.01	0.002	0.01	0.001	0.01	2	1	0.66	0.71	2	0.1	1	1	0.1	0.331	0.084

Table 3. Variation of skin friction (Continued)

t	Kn	τ_q	τ_T	λ_q	λ_C	D	Kc	Sc	Pr	N	Da	M	γ	α	τ_0	$-\tau_1$
0.1	0.01	0.01	0.01	0.001	0.01	2	1	0.66	0.71	2	0.1	1	1	0.1	0.330	0.081
0.1	0.01	0.001	0.02	0.001	0.01	2	1	0.66	0.71	2	0.1	1	1	0.1	0.330	0.0830
0.1	0.01	0.001	0.06	0.001	0.01	2	1	0.66	0.71	2	0.1	1	1	0.1	0.327	0.0831
0.1	0.01	0.001	0.01	0.002	0.01	2	1	0.66	0.71	2	0.1	1	1	0.1	0.3317	0.084
0.1	0.01	0.001	0.01	0.01	0.01	2	1	0.66	0.71	2	0.1	1	1	0.1	0.3319	0.083
0.1	0.01	0.001	0.01	0.001	0.02	2	1	0.66	0.71	2	0.1	1	1	0.1	0.332	0.085
0.1	0.01	0.001	0.01	0.001	0.06	2	1	0.66	0.71	2	0.1	1	1	0.1	0.334	0.089
0.1	0.01	0.001	0.01	0.001	0.01	3	1	0.66	0.71	2	0.1	1	1	0.1	0.354	0.097
0.1	0.01	0.001	0.01	0.001	0.01	4	1	0.66	0.71	2	0.1	1	1	0.1	0.376	0.111
0.1	0.01	0.001	0.01	0.001	0.01	2	2	0.66	0.71	2	0.1	1	1	0.1	0.330	0.083
0.1	0.01	0.001	0.01	0.001	0.01	2	4	0.66	0.71	2	0.1	1	1	0.1	0.327	0.081
0.1	0.01	0.001	0.01	0.001	0.01	2	1	0.22	0.71	2	0.1	1	1	0.1	0.342	0.108
0.1	0.01	0.001	0.01	0.001	0.01	2	1	1.5	0.71	2	0.1	1	1	0.1	0.321	0.069
0.1	0.01	0.001	0.01	0.001	0.01	2	1	0.66	0.9	2	0.1	1	1	0.1	0.322	0.076
0.1	0.01	0.001	0.01	0.001	0.01	2	1	0.66	1	2	0.1	1	1	0.1	0.317	0.073
0.1	0.01	0.001	0.01	0.001	0.01	2	1	0.66	0.71	3	0.1	1	1	0.1	0.523	0.103
0.1	0.01	0.001	0.01	0.001	0.01	2	1	0.66	0.71	4	0.1	1	1	0.1	0.427	0.122
0.1	0.01	0.001	0.01	0.001	0.01	2	1	0.66	0.71	2	0.2	1	1	0.1	0.348	0.093
0.1	0.01	0.001	0.01	0.001	0.01	2	1	0.66	0.71	2	0.4	1	1	0.1	0.354	0.097
0.1	0.01	0.001	0.01	0.001	0.01	2	1	0.66	0.71	2	0.1	2	1	0.1	0.329	0.082
0.1	0.01	0.001	0.01	0.001	0.01	2	1	0.66	0.71	2	0.1	4	1	0.1	0.323	0.079
0.1	0.01	0.001	0.01	0.001	0.01	2	1	0.66	0.71	2	0.1	1	2	0.1	0.257	0.076
0.1	0.01	0.001	0.01	0.001	0.01	2	1	0.66	0.71	2	0.1	1	3	0.1	0.173	0.062
0.1	0.01	0.001	0.01	0.001	0.01	2	1	0.66	0.71	2	0.1	1	1	0.2	0.289	0.067
0.1	0.01	0.001	0.01	0.001	0.01	2	1	0.66	0.71	2	0.1	1	1	0.3	0.175	0.055

4. Conclusion

In this investigation, the Dual-Phase-Lag and diffusion-thermo effects on time-dependent MHD second-grade double-diffusive flow in a fully developed microchannel filled with porous material in the presence of chemical reaction is analyzed. The governing equations of fluid velocity, temperature and concentration are solved using the Laplace transform method the inversion is done numerically using the INVLAP subroutine of MATLAB. It is noticed that the difference between the classical Fourier's heat conduction model, the Cattaneo-Vernotte (CV) model and the Dual-Phase-Lag (DPL) model reduces as time increases. After a dimensionless time span of t=0.5, all the models converge to produce the same result. Hence, in this regard, the flow characteristics of the problem are studied for t=0.1, i.e. where the actual effects of the DPL model could be captured. We found that fluid velocity and fluid temperature decrease as retardation time and thermal relaxation time increase within the microchannel. Species concentration and fluid velocity increase with the increase in phase lag in the concentration gradient while they decrease with the increase in phase lag in the mass flux. Increasing the Dufour number, permeability parameter, Knudsen number increases fluid velocity while magnetic parameter, second-grade parameter and chemical reaction parameter decrease fluid velocity. Chemical reaction reduces species concentration while it enhances fluid velocity. It is deemed that this problem will act as a benchmark for further investigations in the non-Fourier heat and mass transfer mechanisms in the second grade-fluid flows which are indeed very common in polymer industries.

Acknowledgments

The authors would like to thank the skilled reviewers for their valuable suggestions/comments which have helped significantly in enhancing the quality of the manuscript.

Conflict of Interest

The author(s) declared no potential conflicts of interest with respect to the research, authorship and publication of this article.

Funding

The author(s) received no financial support for the research, authorship and publication of this article.

References

[1] Ouellette, J., *An-Ti-Ci-Pa-Tion: The Physics of Dripping Honey*, Scientific America, 2013.

[2] Hayat, T., Saif, S., Abbas, Z., The influence of heat transfer in an MHD second grade fluid film over an unsteady stretching sheet, *Physics letters A*, 372, 2008, 5037-5045.

[3] Hayat, T., Ahmed, N., Sajid, M., Asghar, S., On the MHD flow of a second grade fluid in a porous channel, *Computers and Mathematics with Applications*, 54, 2007, 407-414.

[4] Hayat, T., Abbas, Z., Heat transfer analysis on the MHD flow of a second grade fluid in a channel with porous medium, *Chaos, Solitons and Fractals*, 38, 2008, 556-567.

[5] Das, K., Sharma, R.P., Sarkar, A., Heat and mass transfer of a second grade magnetohydrodynamic fluid over a convectively heated stretching sheet, *Journal of Computational Design and Engineering*, 3, 2016, 330-336.

[6] Babu, D.D., Venkateswarlu, S., Reddy, E.K., Heat and Mass Transfer on MHD Free convective flow of Second grade fluid through Porous medium over an infinite vertical plate, *In IOP Conference Series*, *Materials Science and Engineering*, 225, 2017, 012267.

[7] Cortell, R., MHD flow and mass transfer of an electrically conducting fluid of second grade in a porous medium over a stretching sheet with chemically reactive species, *Chemical Engineering and Processing: Process Intensification*, 46, 2007, 721-728.

[8] Sheikholeslami, M., Influence of magnetic field on Al2O3-H2O Nanofluid forced convection heat transfer in a porous lid driven cavity with hot sphere obstacle by means of LBM, Journal *of Molecular Liquids*, 263, 2018, 472-488.

[9] Sheikholeslami, M., Application of Darcy law for Nanofluid flow in a porous cavity under the impact of Lorentz forces, *Journal of Molecular Liquids*, 266, 2018, 495-503.

[10] Sheikholeslami, M., Solidification of NEPCM under the effect of magnetic field in a porous thermal energy storage enclosure using CuO Nanoparticles, *Journal of Molecular Liquids*, 263, 2018, 303-315.

[11] Sheikholeslami ,M., Shehzad, S.A., Li, Z., Shafee, A., Numerical modeling for alumina Nanofluid Magnetohydrodynamic convective heat transfer in a permeable medium using Darcy law, *International Journal of Heat and Mass Transfer*, 127, 2018, 614-622.

[12] Sheikholeslami ,M., Li, Z., Shafee, A., Lorentz forces effect on NEPCM heat transfer during solidification in a porous energy storage system, *International Journal of Heat and Mass Transfer*, 127, 2018, 665-674.

[13] Sheikholeslami, M., Shehzad, S.A., Li, Z., Water based Nanofluid free convection heat transfer in a three dimensional porous cavity with hot sphere obstacle in existence of Lorenz forces, *International Journal of Heat and Mass Transfer*, 125, 2018, 375-386.

[14] Sheikholeslami, M., Houman, B.R., Simulation of Nanofluid heat transfer in presence of magnetic field: a review, *International Journal of Heat and Mass Transfer*, 115, 2017, 1203-1233.

[15] Makinde, O.D., Khan, Z.H., Ahmad, R., Khan, W.A. Numerical study of unsteady hydromagnetic radiating fluid flow past a slippery stretching sheet embedded in a porous medium, *Physics of Fluids*, 30(8), 2018, 083601.

[16] Makinde, O.D., Sandeep, N., Ajayi, T.M., Animasaun, I.L., Numerical exploration of heat transfer and Lorentz force effects on the flow of mhd casson fluid over an upper horizontal surface of a thermally stratified melting surface of a paraboloid of revolution, *International Journal of Nonlinear Sciences and Numerical Simulation*, 19(2-3), 2018, 93-106.

[17] Makinde, O.D., Reddy, M.G., Reddy, K.V., Effects of thermal radiation on MHD peristaltic motion of Walters-b fluid with heat source and slip conditions, *Energy*, 5(6), 2017, 7.

[18] Sarkar, S., Seth, G.S., Unsteady Hydromagnetic Natural convection flow past a vertical plate with time-dependent free stream through a porous medium in the presence of Hall current, rotation, and heat absorption, *Journal of Aerospace Engineering*, 30(1), 2016, 04016081.

[19] Seth, G.S., Sarkar, S., Chamkha, A.J., Unsteady hydromagnetic flow past a moving vertical plate with convective surface boundary condition, *Journal of Applied Fluid Mechanics*, 4, 2016, 1877-1886.

[20] Seth, G.S., Sarkar, S., Makinde, O.D., Combined free and forced convection Couette-Hartmann flow in a rotating channel with arbitrary conducting walls and Hall effects, *Journal of Mechanics*, 32(5), 2016, 613-629.

[21] Seth, G.S., Kumbhakar, B., Sarkar, S., Unsteady MHD natural convection flow with exponentially accelerated free-stream past a vertical plate in the presence of Hall current and rotation, *Rendiconti del Circolo Matematico di Palermo Series* 2, 66(3), 2017, 263-283.

[22] Kandlikar, S., Garimella, S., Li, D., Colin, S., King, M.R., *Heat transfer and fluid flow in minichannels and microchannels* Elsevier, 2005.

[23] Shen, C., *Rarefied gas dynamics: fundamentals, simulations and micro flows*, Springer Science and Business Media, 2006.

[24] Misra, J.C., Chandra, S., Electro-osmotic flow of a second-grade fluid in a porous microchannel subject to an AC electric field, *Journal of Hydrodynamics,* 25*,* 2013, 309-316.

[25] Chen, C.K., Weng, H.C., Developing natural convection with thermal creep in a vertical microchannel, *Journal of Physics D: Applied Physics*, 39, 2006, 3107–3118.

[26] Hooman, K., Heat and fluid flow in a rectangular microchannel filled with a porous medium, *International Journal of Heat and Mass Transfer*, 51, 2008, 5804-5810.

[27] Buonomo, B., Manca, O., Natural convection slip flow in a vertical microchannel heated at uniform heat flux, *International Journal of Thermal Sciences*, 49, 2010, 1333-1344.

[28] Jha, B.K., Aina, B., Joseph, S.B., Natural convection flow in a vertical microchannel with suction/injection, Proceedings of the Institution of Mechanical Engineers, Part E: Journal of Process of Mechanical Engineering, 228, 2014,171-180.

[29] Hetsroni, G., Mosyak, A., Pogrebnyak, E., Yarin, L.P., Fluid flow in micro-channels, *International Journal of Heat and Mass Transfer*, 48, 2005, 1982-1998.

[30] Das, S., Jana, R.N., Makinde, O.D., Mixed convective magnetohydrodynamic flow in a vertical channel filled with nanofluids, *Engineering Science and Technology, an International Journal*, 18, 2015, 244-255.

[31] Zhang, Z. M., *Nano/Microscale Heat Transfer*, McGraw Hill, New York, 2007.

[32] Catteneo, C., A form of heat conduction equation which eliminates the paradox of instantaneous propagation, *Compte Rendus*, 247, 1958, 431–433.

[33] Vernotte, P., Some possible complications in the phenomena of thermal conduction, *Compte Rendus*, 252, 1961, 2190-2201.

[34] Khadrawi, A.F., Othman, A., Al-Nimr, M.A., Transient free convection fluid flow in a vertical microchannel as described by the hyperbolic heat conduction model, *International Journal of Thermophysics*, 26, 2005, 905-918.

[35] Choi, J.H., Yoon, S.H., Park, S.G., Choi, S.H., Analytical solution of the Cattaneo-Vernotte equation (non-Fourier heat conduction), *Journal of Korean Society of Marine Engineering*, 40, 2016, 389-396.

[36] Tzou, D.Y., The generalized lagging response in small-scale and high-rate heating, *International Journal of Heat and Mass Transfer*, 38, 1995b, 3231-3240.

[37] Tzou, D.Y., *Macro-to microscale heat transfer: the lagging behavior,* John Wiley and Sons, 2014.

[38] Sobhan, C.B., Peterson, G.P., *Microscale and nanoscale heat transfer: Fundamental of Engineering and Applications*, CRC Press, 2008.

[39] Khadrawi, A.F., Al-Nimr, M.A., Unsteady natural convection fluid flow in a vertical microchannel under the effect of the dual-phase-lag heat-conduction model, *International Journal of Thermophysics*, 28, 2007, 1387-400.

[40] Ajibade, A.O., Dual-phase-lag and Dufour effects on unsteady double-diffusive convection flow in a vertical microchannel filled with porous material, *Proceedings of the Institution of Mechanical Engineers, Part E: Journal of Process Mechanical Engineering*, 228, 2014, 272-285.

[41] De Hoog, F.R., Knight, J.H., Stokes, A.N., An improved method for numerical inversion of Laplace transforms, *SIAM Journal on Scientific and Statistical Computing*, 3, 1982, 357-366.

[42] Hollenbeck, K.J., A matlab function for numerical inversion of Laplace transforms by the de Hoog algorithm, http://www. isva. dtu. dk/staff/karl/invlap.htm, 1998.

Appendix A

$$k_1 = 1 - \frac{Kn\sqrt{q}}{S_c}, k_2 = 1 + \frac{Kn\sqrt{q}}{S_c}, k_3 = 1 - \frac{Kn\sqrt{P}}{P_r}, k_4 = 1 + \frac{Kn\sqrt{P}}{P_r}, k_5 = 1 - \frac{Kn\sqrt{q}}{P_r}, k_6 = 1 + \frac{Kn\sqrt{q}}{P_r}, \tag{A1}$$

$$k_7 = C_3 e^{-\sqrt{P}} + C_4 e^{\sqrt{P}} + C_5 e^{\sqrt{q}} + C_6 e^{-\sqrt{q}}, k_8 = Kn\left(\sqrt{P}\left(C_3 e^{-\sqrt{P}} - C_4 e^{\sqrt{P}}\right) + \sqrt{q}\left(C_6 e^{-\sqrt{q}} - C_5 e^{\sqrt{q}}\right)\right) \tag{A2}$$

$$A_1 = (1 - A_2 s k_2) s^{-1} k_1^{-1}, A_2 = k_2 e^{\sqrt{q}}\left(k_2^2 e^{\sqrt{q}} - k_1^2 e^{-\sqrt{q}}\right)^{-1} s^{-1}, B_1 = \left(s^{-1} - B_2 k_3 - B_3 k_5 - B_4 k_6\right) k_4^{-1} \tag{A3}$$

$$B_2 = \left(\left(s^{-1} - B_3 k_5 - B_4 k_6\right) k_3 e^{-\sqrt{P}} + B_3 k_4 k_6 e^{\sqrt{q}} + B_4 k_4 k_5 e^{-\sqrt{q}}\right)\left(k_3^2 e^{-\sqrt{P}} - k_4^2 e^{\sqrt{P}}\right)^{-1} \tag{A4}$$

$$B_3 = \frac{DA_1 q}{(1 + s\tau_T)(P - q)}, B_4 = \frac{DA_2 q}{(1 + s\tau_T)(P - q)} \tag{A5}$$

$$h_1 = Kn\sqrt{R} - 1, h_2 = Kn\sqrt{R} + 1, h_3 = Kn\sqrt{P} - 1, h_4 = Kn\sqrt{P} + 1, h_5 = Kn\sqrt{q} - 1, h_6 = Kn\sqrt{q} + 1 \tag{A6}$$

$$h_7 = h_1 e^{-\sqrt{R}}, h_8 = -h_2 e^{\sqrt{R}}, h_9 = h_1 h_2^{-1}, \quad C_1 = \left(C_2 h_1 - C_3 h_4 + C_4 h_3 + C_5 h_5 - C_6 h_6\right) h_2^{-1}, \tag{A7}$$

$$C_2 = \left[h_2(k_7 - k_8) + (C_3 h_4 - C_4 h_3 - C_5 h_5 + C_6 h_6) h_7\right]\left[h_2(h_8 + h_7 h_9)\right]^{-1}, C_3 = B_1\left(\gamma(R - P)\right)^{-1}, C_4 = B_2\left(\gamma(R - P)\right)^{-1} \tag{A8}$$

$$C_5 = (B_3 + NA_1)\left(\gamma(R - q)\right)^{-1}, C_6 = (B_4 + NA_2)\left(\gamma(R - q)\right)^{-1} \tag{A9}$$